

# SUPERCONDUCTING RF FOR THE CORNELL ENERGY-RECOVERY-LINAC MAIN LINAC \*

M. Liepe<sup>†</sup>, Y. He, G. Hoffstaetter, S. Posen, J. Sears, V. Shemelin, M. Tigner, V. Veshcherevich, N. Valles CLASSE, Cornell University, Ithaca, NY 14853, USA

## Abstract

Cornell University is developing the superconducting RF technology required for the construction of a 100 mA hard X-ray light source driven by an Energy-Recovery Linac. Prototype components of the 5 GeV cw SRF main linac cryomodule are under development and fabrication. This work includes an optimized 7-cell SRF cavity, a cold frequency tuner, a broadband HOM beamline absorber, and a 5 kW cw RF input coupler. A Horizontal Test Cryostat (HTC) is also under design, and will be used for a first horizontal test of the ERL main linac cavity in 2012 and later for a beam test of the cavity at high beam current. In this paper we give an overview of these activities at Cornell.

## INTRODUCTION

Continuous progress in Superconducting Radio-Frequency (SRF) technology during the last three decades had transformational impact on particle accelerators for many different applications. Multi-GeV SRF linacs running in CW mode and supporting beam currents of tens of mA are now coming into reach, which will enable novel high current accelerators like an x-ray light source based on the Energy-Recovery-Linac (ERL) principle. Such an accelerator is currently under development at Cornell University's Laboratory for Accelerator based Sciences and Education [1].

After fabrication and successful commissioning and testing of a short SRF linac section in the ERL injector prototype at Cornell [2], the main focus is now on developing the SRF technology for the 5 GeV ERL main linac, supporting beam currents exceeding  $2 \times 100$  mA (100 mA in the accelerated beam and 100 mA in the decelerated beam). Fig. 1 shows the layout of the Cornell ERL design and Table 1 summarizes the specifications for the SRF main linac. After fully developing and testing the individual main linac beam line components, a single cavity test cryomodule will be fabricated and tested first before a full main linac prototype cryomodule hosting six 7-cell cavities will be fabricated at Cornell.

## ERL MAIN LINAC

The 5 GeV Cornell ERL main linac will have 384 7-cell SRF cavities, running CW at 16.2 MV/m accelerating gradient. Each main linac cryomodule will host 6 SRF cavi-

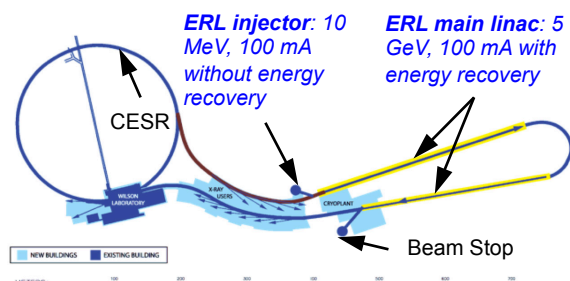


Figure 1: Layout of the Cornell ERL. The 5 GeV main linac would consist out of two continuous linac sections located in a new tunnel which would extend the existing CESR tunnel.

ties; see Fig. 2 and Tables 1 and 2. Key challenges that need to be addressed in the main linac cryomodule include: (1) Support of CW cavity operation with high dynamic cryogenic loads, (2) supporting high beam current ERL operation up to  $2 \times 100$  mA with short (2 ps) bunches, and (3) operating the SRF cavities at a high loaded quality factor  $Q_L \geq 6.5 \times 10^7$  while still achieving excellent RF field stability.

## ERL MAIN LINAC CAVITY

The 7-cell main linac cavities are optimized for a high  $R/Q$  of the fundamental mode of  $387 \Omega$  (circuit definition) and for strong HOM damping by optimizing the shape of the end cells [3]. Fig. 3 shows the optimized cavity, and Table 3 lists some of its parameters. HOMs up to 10 GHz

Table 1: Cornell ERL main linac specifications

Parameter	Value
Total energy gain	5 GeV
max. beam current	100mA
Bunch charge	77pC
Bunch length	2ps
Number of linacs	2
Modules per linac	35 (linac A); 29 (linac B)
Linac length	344 (linac A); 285 (linac B)
Cavities per module	6
Total number of cavities	384
Linac fill factor	49%

\* Work supported by NSF award DMR-0807731.

<sup>†</sup> MUL2@cornell.edu

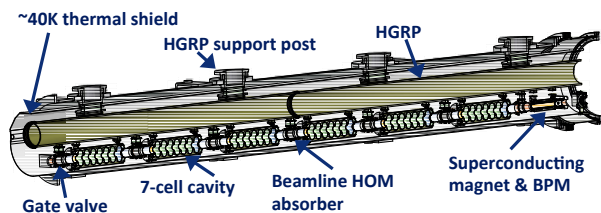


Figure 2: Cross-section of the ERL main linac module with six SRF cavities and HOM beamline absorbers in between. A superconducting magnet package is located at the end of the module.

in frequency were calculated taking into account realistic material properties of the RF absorbing rings in the HOM beamline dampers, see Fig. 4. Robustness of the obtained cavity design to small shape imperfections was verified by calculating HOMs in deformed cavity shapes, resulting in a tolerance specification for the cavity cell shape of  $\pm 0.25$  mm. Beam-break-up (BBU) simulations were done taking into account the strongest dipole modes found in HOM calculations for the 7-cell cavity shape with realistic RF absorber materials, see Fig. 5. As can be seen, larger variation in the cavity to cavity HOM frequencies leads to a larger BBU current, since it reduces the likelihood of coherent excitation of a given HOM in multiple cavities by the beam. While relaxed cavity shape tolerances would increase the HOM frequency spread, they also increase the risk of trapped HOMs which can result in a drastic reduction in the BBU current (see for example the threshold current found for the  $\pm 1$  mm case in Fig. 5). Cornell's solution is using several classes of cavities in the main linac, which are small, controlled variations of the baseline 7-cell cavity design [3]. This approach allows increasing the HOM frequency spread significantly to  $\sigma_f/f > 4 \times 10^{-3}$ , thereby increasing the BBU current to  $> 400$  mA, while still preserving the optimized properties of the accelerating mode.

The mechanical design of the cavity was optimized for low microphonics by placing stiffening rings between the cells. Selecting an ideal radial position of these rings reduces the sensitivity of the fundamental mode frequency to changes in the LHe bath pressure (see Fig. 6), which is a main source of cavity microphonics.

A first prototype Niobium cavity is completed, see Fig. 3, and is currently under preparation for a first vertical test. Measurements of the half cell shape after deep drawing by a coordinate measurement machine were used to correct the profile of the deep drawing dies for spring back of the Niobium; see Fig. 7. These measurements showed that the shape errors are within the  $\pm 0.25$  mm specification discussed above. Frequency measurements of welded dumbbells were used to find final trim amounts for the equators prior to the equator welds. After fabrication, and before any field flatness tuning, the cavity had a field flatness of  $\approx 90\%$ , which confirms excellent control of the cell shape throughout the entire cavity fabrication process.

## RF INPUT COUPLER

The input couplers for Cornell Energy Recovery Linac must deliver up to 5 kW CW RF power to the main linac cavities, though under nominal conditions they will operate with 2 kW average and 5 kW peak power. Due to the principles of energy recovery in a superconducting cavity, the couplers will operate under conditions with full reflection for the great majority of the time and thus require active cooling of the inner conductor. To make the design more economical, the couplers will provide fixed coupling to the cavities. Coupling adjustability can be achieved using three-stub tuners in the feed-transmission line to have a range of  $2 \times 10^7$  to  $1 \times 10^8$ , with the nominal operational  $Q_{ext} = 6.5 \times 10^7$ . The design of the ERL main linac coupler is based on the TTF-III and Cornell ERL injector couplers [7], and takes into account experience gained from the ERL injector couplers. A CAD model of the main linac coupler is shown in Fig. 8. The ERL linac couplers

Table 2: Main linac cryomodule specifications

Parameter	Value
Number of cavities	6
Number of cells per cavity	7
Accelerating gradient	16.2MV/m
Fundamental mode frequ.	1.3GHz
Loaded quality factor	$6.5 \times 10^7$
Couplers per cavity	1
RF power per cavity	5kW
Required amp.. stab. (rms)	$2 \times 10^{-4}$
Required phase stab. (rms)	$0.1^\circ$
Number of HOM loads	7
HOM per per cavity	W
Design beam current	2x100mA
Total 2K / 5K / 80K loads	76/70/1500W
Overall length	9.8m

Table 3: Main linac SRF cavity specifications

Parameter	Value
Fundamental mode frequ.	1.3GHz
Accelerating gradient	16.2MV/m
Intrinsic quality factor	$\geq 2 \times 10^{10}$
Loaded quality factor	$6.5 \times 10^7$
Active length	0.91m
Cell-to-cell coupling	2.2%
Iris diameter	72mm
Beam tube diameter	110mm
R/Q (circuit definition)	$387\Omega$
Geometry factor	$271\Omega$
$E_{peak}/E_{acc}$	2.06
$H_{peak}/E_{acc}$	4.2mT/(MV/m)
Long. loss factor	13.2V/pC

must accommodate lateral movement of the cavities during cool-down of up to 5 mm, since one end of the coupler is attached to the moving cavity and the other end is attached to the fixed vacuum vessel port. Two sets of bellows are placed on the warm portion of the coupler, on both the inner conductor and on the outer conductor, as shown in Fig. 8. In this way, high flexibility is achieved while keeping the cold antenna fixed relative to the cavity coupler port.

## COLD TUNER

The modified version of the Saclay I tuner [8] was chosen for the ERL linac. An illustration of the modified tuner is shown in Fig. 9. The bore diameter was increased to fit over a larger diameter beam tube of the ERL 7-cell cavity. The tuner frame and the piezo stacks were modified for increase stiffness to support high tuner forces of up to 26 kN for the main linac cavity version with stiffening rings. ANSYS simulations confirm that the modified version of the tuner can supply the required tuning force, see Fig. 9.

## HOM DAMPER

The Higher Order Mode (HOM) loads in the ERL main linac cryomodule are intimately linked to the SRF cavity design and mitigation of the beam breakup instability (BBU) as described above. The average HOM power is expected to be 200 W per cavity. Most of the power will be in the few GHz frequency range, but the short ERL bunch length will allow HOM spectral content up to the 100 GHz range. The HOM damping scheme must then have strong coupling over this broad bandwidth and be able to dissipate the high average power.

Beamline loads located between the cavities were chosen to provide broadband HOM damping in the ERL main linac; see also Fig. 2. The beamline loads are conceptually straightforward, where HOMs propagate as TE or TM modes in the circular beampipe and are heavily damped at the absorber. This provides broadband damping with only modest dependence on the RF absorber properties and no need for careful geometrical tuning of coupling structures. To avoid an undue load on the refrigeration plant from the expected 200 W of HOM power, the RF absorber

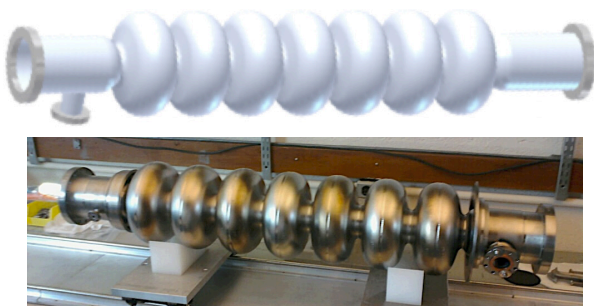


Figure 3: Top: CAD model of the 7-cell ERL main linac cavity. Bottom: Finished Niobium 7-cell prototype cavity.

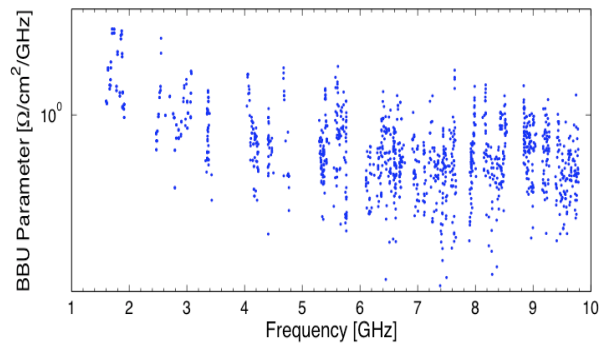


Figure 4: BBU parameter  $(R/Q)\sqrt{Q}/f$  vs. frequency for all dipole HOMs up to 10 GHz in the 7-cell ERL main linac cavity [4]. The parameters of the HOMs were calculated with the 2-dimensional code CLANS for SiC based beam-line HOM absorbers located between the cavities.

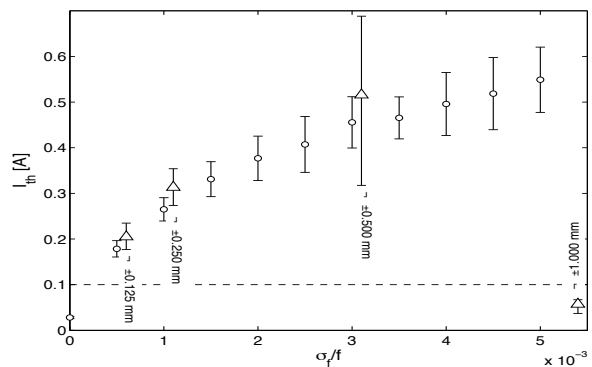


Figure 5: BBU threshold current versus frequency spread (BMAD simulations) [5]. Circular shaped symbols: BBU current for the HOM spectrum of the optimized cavity with HOM frequency spread introduced artificially in the beam tracking simulation. Triangular shaped symbols: BBU mean values for realistic ERLs, in which each cavity has unique, small shape imperfections of the size listed in the graph. The shape imperfections then result in the HOM frequency spread between cavities shown. The error bars mark the lowest and highest current obtained by the middle 80% of the runs.

is maintained at 100 K and thus necessitates thermal gradients along the beamline between cavities. The thermal gradient is defined by a 5 K intercept between the 1.8 K cavity and the 100 K HOM absorber.

A CAD model of the ERL main linac beamline HOM load is shown in Fig. 10. The design is based on the ERL injector HOM beamline load, but with significant simplifications. The load has an RF absorber as a unitary cylinder brazed into a metal sink, and stainless-steel bellows for flexibility of flange alignment. The RF absorber cylinder is extending along the bellows to shield the bellows from the beam and to damp high-frequency trapped modes in the bellow sections.

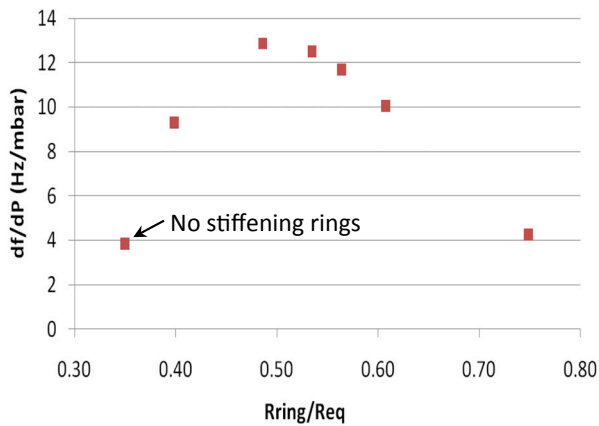


Figure 6: Sensitivity of the fundamental mode frequency to small changes in the LHe bath pressure vs. radius of the stiffening rings between the cells (ANSYS simulations). [6]



Figure 7: Verification of cell shape. Left: Coordinate measurement machine (CMM) scanning of half cells. Middle: CMM results show that cell shape errors are within 0.125 mm after deep drawing. Right: Frequency check of finished dumbbells used to determine equator trim dimensions for correct frequency.

Candidates the the RF-absorbing material that have the requisite properties have been studied in detail and full scale samples are in hand. The prototype HOM loads will use a graphite loaded SiC material, which has strong, broadband losses and sufficient DC conductivity to avoid charging up by the beam. Cleaning tests of this material have shown very good performance.

### RF AND LLRF

Each main linac cavity will be driven by its individual 5 kW CW RF source to maximize flexibility in adjusting operating parameters and to support stable operation in the presence of microphonics levels of the order of a cavity bandwidth. In ERL cavity operation with no effective beam loading, efficient cavity operation and minimization of the peak RF power is achieved by operating the cavity at a half bandwidth equal to the maximum peak detuning expected. Assuming a cavity detuning of 10 Hz thus gives a high opti-

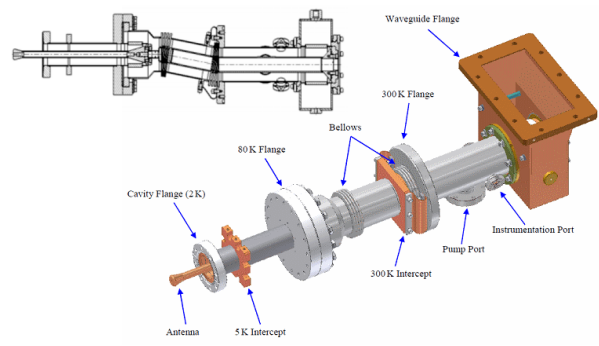


Figure 8: Main linac fixed RF input coupler. Top left corner: The ERL linac input coupler is mechanically flexible, yet maintains alignment of the cavity antenna.

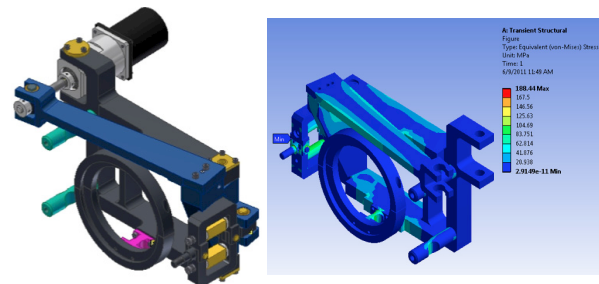


Figure 9: Modified SACLAY I tuner with fast piezoelectric actuators and increased stiffness for the main linac cavities. Left: CAD model. Right: ANSYS simulation of the von-Mises stress for a tuning force of 26 kN applied to the cavity. The maximum stress is well below the yield strength of stainless steel at cryogenic temperatures.

mal loaded quality factor of  $6.5 \times 10^7$ . Without Low-Level RF (LLRF) field control, microphonics would cause very large field perturbation under these conditions (tens of % in amplitude and tens of degree in phase), whereas excellent RF field stability will be required for the operation of an ERL as an X-ray light source.

Cornell has developed a powerful LLRF control system based on digital technology with very low loop latency

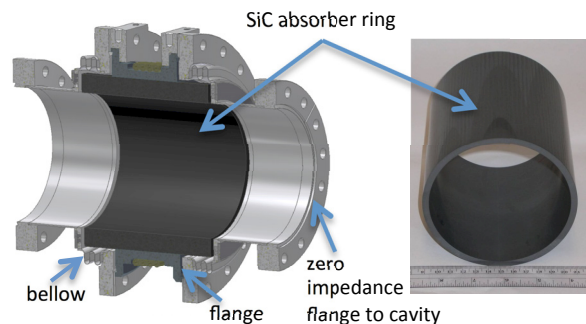


Figure 10: HOM beamline load for the ERL main linac. Left: CAD model cross section. Right: SiC absorber ring.

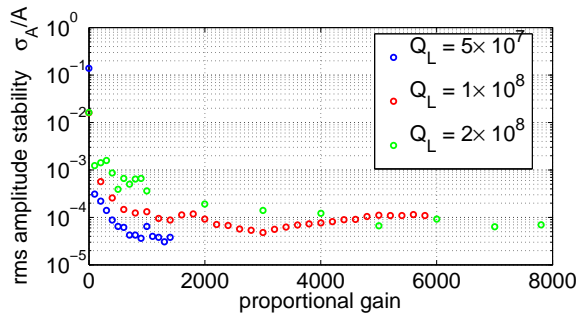


Figure 11: Measured RF field amplitude stability vs. proportional gain for a 9-cell cavity operated at different loaded quality factors in presence of  $\approx 30$  Hz peak microphonics.

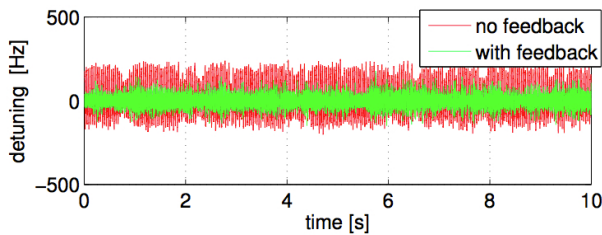


Figure 12: Microphonics compensation by a fast piezoelectric tuner in feedback mode for one of the 2-cell SRF cavities at the Cornell ERL injector SRF cryomodule.

$< 1 \mu\text{s}$ . Tests of this LLRF control system at a test cryomodule hosting an ILC 9-cell cavity at the Helmholtz-Zentrum Berlin have shown that excellent RF field stability can be achieved even at record high loaded quality factors of  $Q_L = 2 \times 10^8$  and in presence of very strong field perturbations by cavity microphonics exceeding several cavity bandwidths; see Fig. 11. Lower microphonics levels result in lower RF power required to operate a cavity at a given field gradient. The potential of actively reducing microphonics was successfully demonstrated at one of the ERL injector cavities, reducing the rms microphonics by as much as 70% as shown in Fig. 12.

## SC MAGNET

Each linac cryomodule will contain one quadrupole with adjacent horizontal and vertical steering coils. A iron yoke magnet design has been selected for the quadrupole since the relatively low gradient can be realized with a conventional iron-based design using superconducting coils, allowing the quadrupole to utilize the 1.8 K liquid helium available in the cryomodule. A CAD model of the yoke and coils is shown in Fig. 13. The stray magnetic field from the magnet package was carefully minimized inside of the cryomodule to maintain a high SRF cavity  $Q_0$ . At a distance of 15 cm from the edge of the yoke, the unshielded stray field is  $\approx 65$  mG. Cryogenic magnetic shielding will be wrapped around the magnet package to reduce this number

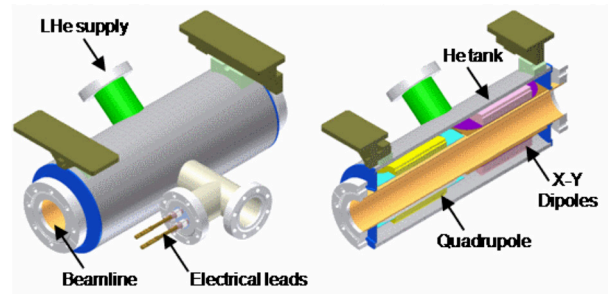


Figure 13: The superconducting quadrupole and dipole magnets in their helium vessel with the HTS leads. The field gradient at 2.5 A is 0.00437 T/m.

further. For the dipole corrector, a single-layer coil is chosen similar to that for the quadrupole. However, the dipole coil is placed inside of the iron yoke as this gives minimal stray fields outside of the corrector.

## MODULE DESIGN

The main linac module design is based on the successful injector module, employing many of the innovations developed for the injector module [2, 9]. A longitudinal cross section of the main linac module is shown in Fig. 2. The cavities are supported by a large diameter Helium-gas return pipe (HGRP), and all cryogenic manifolds are located inside the cryomodule, as was originally developed for the TTF cryomodules at DESY. The Cornell module design includes novel features like (1) access ports in the vacuum vessel allowing accessing the frequency tuners without removing the cold mass from the module, (2) a rail system inside the vacuum vessel to slide the cold mass into the vacuum vessel, (3) gate valves at the module ends with actuators located outside of the module, and (4) high precision supports for the beamline components hanging from the HGRP. The fixed, high precision cavity supports are also used in the Cornell injector cryomodule, and have been shown to significantly simplify the module assembly and to result in excellent alignment of the beam line components. Refer to Figs. 14 and 15 for more details on these module design features. The cryogenic manifolds inside the cryomodule are sized to handle the substantial cryogenic loads in CW cavity operation with high beam currents. Fig. 16 shows the conceptual layout of the 1.8K system inside each module. The 2-phase line is connected to the HGRP in the middle of the module to minimize the gas flow velocity in the 2-phase line. The liquid Helium level in each module is controlled independently via a JT-valve. Three layers of magnetic shields will be used to achieve very low residual magnetic fields at the cavity locations to support intrinsic quality factors of the SRF cavities of  $Q_0 \geq 2 \times 10^{10}$ . A  $\approx 40$ K shield intercepts thermal radiation from the vacuum vessel at room temperature. Cost studies have shown that an additional 5K shield is not economical for SRF cryomodules operated in CW mode at medium field gradients.

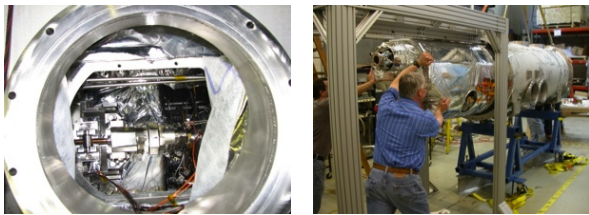


Figure 14: Left: Tuner motor access port in the vacuum vessel of the Cornell ERL injector SRF cryomodule before closing it. Right: Sliding of the cold mass of the injector cryomodule into the vacuum vessel, using rails at the top of the vessel. The ERL main linac cryomodule will also include both of these design features.

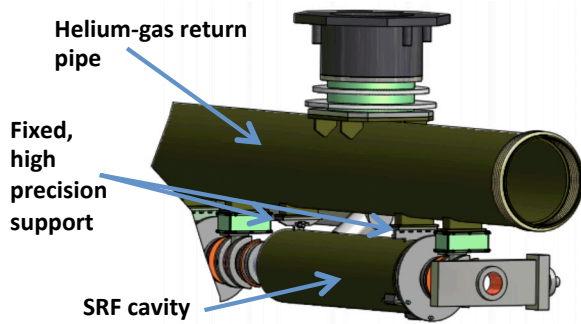


Figure 15: Cavity support in the main linac. The cavities are mounted to the Helium-gas return pipe via fixed, high precision supports, which are determining the transverse and longitudinal position of the cavity.

### TEST MODULE

One of the most critical parameter in the ERL main linac is the average intrinsic quality factor  $Q_0$  of the cavities,

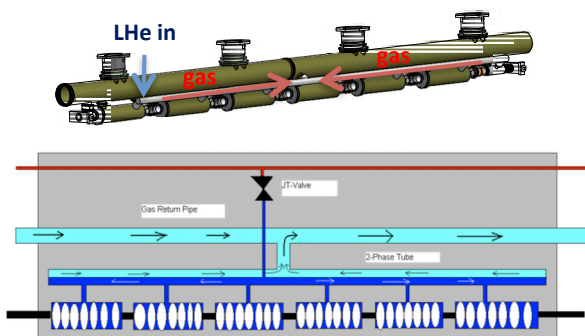


Figure 16: Liquid Helium and Helium gas flow in the main linac cryomodule. A 2-phase line supplies LHe to the individual cavities, and also brings the gas to the Helium-gas return pipe via a connection in the middle of the module.

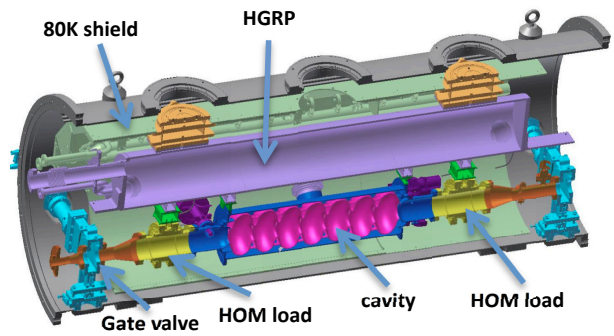


Figure 17: CAD model cross section of the horizontal test cryomodule.

since it determines the dynamic cryogenic load from the cavities, which is dominating in CW cavity operation over all other cryogenic loads. In order to study the intrinsic quality factor achievable in a full cryomodule installation, and potential risks of reducing  $Q_0$  during module assembly, a single cavity test cryomodule is currently under fabrication, see Fig. 17. The cryomodule will be assembled several times with increasing complexity of the beam line (first without high power input couplers and HOM beam-line loads, which will then be included in subsequent assemblies of the test module), and the intrinsic quality factor of the cavity will be measured after each assembly for a systematic study.

### SUMMARY AND OUTLOOK

Cornell is in the process of developing the SRF technology for a multi-GeV, high beam current superconducting main linac. All beamline components meeting the resulting demanding specifications have been developed, including the SRF cavity, RF input coupler, cold frequency tuner, beamline HOM loads, and SC magnets, and are currently under fabrication and testing. A first test of a fully equipped main linac cavity is planned for 2012 in a single cavity test cryomodule. Following the successful completion of this test, a first full main linac prototype cryomodule will be assembled at Cornell and RF tested. A high beam current test of the single cavity module is also planned in the Cornell ERL injector to study the high current performance of the cavity and the HOM damping by the beamline HOM loads.

### REFERENCES

- [1] C. Mayes et al., PAC 2011, New York, USA (2011).
- [2] M. Liepe et al., PAC'05, Knoxville, TN, USA (2005).  
M. Liepe et al., IPAC'11, San Sebastian, Spain (2011).
- [3] N. Valles, M. Liepe, PAC 2011, New York, USA (2011).
- [4] N. Valles, M. Liepe, LINAC 2010, Tsukuba, Japan (2010).
- [5] N. Valles, M. Liepe, SRF 2011, Chicago, IL, USA (2011).
- [6] S. Posen, M. Liepe, SRF 2011, Chicago, IL, USA (2011).

- [7] V. Veshcherevich et al., SRF 2009, Berlin, Germany (2009).
- [8] Bosland, P. and B. Wu, Technical Report CARE-Note-2005-004- SRF, DAPNIA - CEA Saclay (2005).
- [9] E. Chojnacki et al., PAC09, Vancouver, Canada, (2009).